2018 25th International Lightning Detection Conference &
7th International Lightning Meteorology Conference
March 12 - 15 | Ft. Lauderdale, Florida, USA

An electrostatic model of bidirectional leader observed with a high-speed video camera

M. D. Tran* and V. A. Rakov*,†
*Electrical and Computer Engineering Department, University of Florida, Gainesville, Florida, 32611, USA
†Institute of Applied Physics, Russian Academy of Sciences, Nizhny Novgorod, 603950, Russia

***Abstract*—Complete evolution of a lightning discharge, from its initiation at an altitude of about 4 km to its ground attachment, was optically observed, for the first time, at the Lightning Observatory in Gainesville (LOG), Florida (Tran and Rakov, 2016) [1]. During this lightnig flash, a bidirectional leader, whose negative end terminated on the ground and produced a return stroke, was imaged to develop in virgin air for 12 ms. An electrostatic model of this bidirectional leader was developed using the high-speed video images and electric field waveform, all obtained at the LOG. The positive end exhibited small variations in length, while the negative end extended steadily from 4.1 to 1.0 km above the ground level. The maximum line charge density at the negative end was estimated to be -1.6 mC/m, when its length was 4.4 km. At the same time, the maximum line charge density of the positive end was 5.5 mC/m. The charge transfer of the bidirectional leader was 3.3 C, corresponding to an average current of 393 A. If the slope of negative line charge density profile is assumed to remain the same until the leader attachment to ground, the total charge transfer to ground Q will be 5.6 C, which statistically corresponds to a peak current of 35 kA, which is close to 36 kA reported by the National Lightning Detection Network.**

Keywords*—Lightning, initiation, bidirectional leader, recoil leader, electrostatic model, stepped leader, return stroke, high-speed camera.

I. INTRODUCTION

The mechanism of lightning initiation remains unknown despite recent new observations of lightning initiation. It is still not clear how a sustained lightning channel is formed in thunderclouds. Nevertheless, it is well accepted that the sustained leader should extend bidirectionally, although its positive and negative ends may behave differently. Optical observations of bidirectional leaders, which resulted in a new branch of lightning discharge, were reported by Montanya et al. (2015) [2] and Warner et al. (2016) [3]. The only observation of bidirectional leader that made connection to the ground and produced a cloud-to-ground lightning flash was published by Tran and Rakov (2016) [1].

Rison et al. (2016) [4] recently reported on the so-called fast ($> 10^7$ m/s) positive breakdown in virgin air giving rise to narrow bipolar pulses (NBPs), although most of the flashes do not exhibit the NBP-like signature (either wideband or VHF) at their onset. Liu et al. (2017) [5] reported on breakdown waves similar to the fast positive breakdown, both of them propagating at speed of 10^7 m/s and initiating NBPs. Since the propagation direction is opposite to that expected for fast positive breakdowns, these breakdown waves were termed "fast negative breakdown".

For the purpose of computing ground-level electric field, lightning leaders in cloud-to-ground lightning are often modeled as the system consisting of a point charge (cloud charge source) and a downward-extending leader channel (e.g., Rakov and Uman (2003), page 129) [6]. There are attempts to account for the geometry of the positive part of the bidirectional leader, for example, by Mazur and Ruhnke (1993) [7], who assumed it to be vertical.

In this paper, we take advantage of the unique observation of bidirectional leader reported by Tran and Rakov (2016) [1] to develop an electrostatic model with a realistic model geometry inferred from high-speed video images. First, we briefly discuss the context, in which the bidirectional leader giving rise to a cloud-to-ground flash occurred. Then, the electrostatic model and its predicts will be presented and discussed.

II. OVERVIEW OF THE BIDIRECTIONAL LEADER OBSERVATION

Figure 1a shows a composite image of 41 selected frames of the observed cloud-to-ground lightning discharge, which were acquired with the Phantom V310 camera. Tran and Rakov (2016) identified the left end of the bidirectional leader as positive and the right end as negative. The bidirectional-leader seed was first visible 135.2 ms prior to the return-stroke onset, during the late stage of the preceding cloud flash (see Figures 1b and 1c). All times in this paper are related to the return-stroke onset. The lightning seed was formed through intermittent channel illumination for over 100 ms, with bidirectional leader extension unambiguously starting at -13.6 ms (maybe even as early as at -14.9 ms). The bidirectional

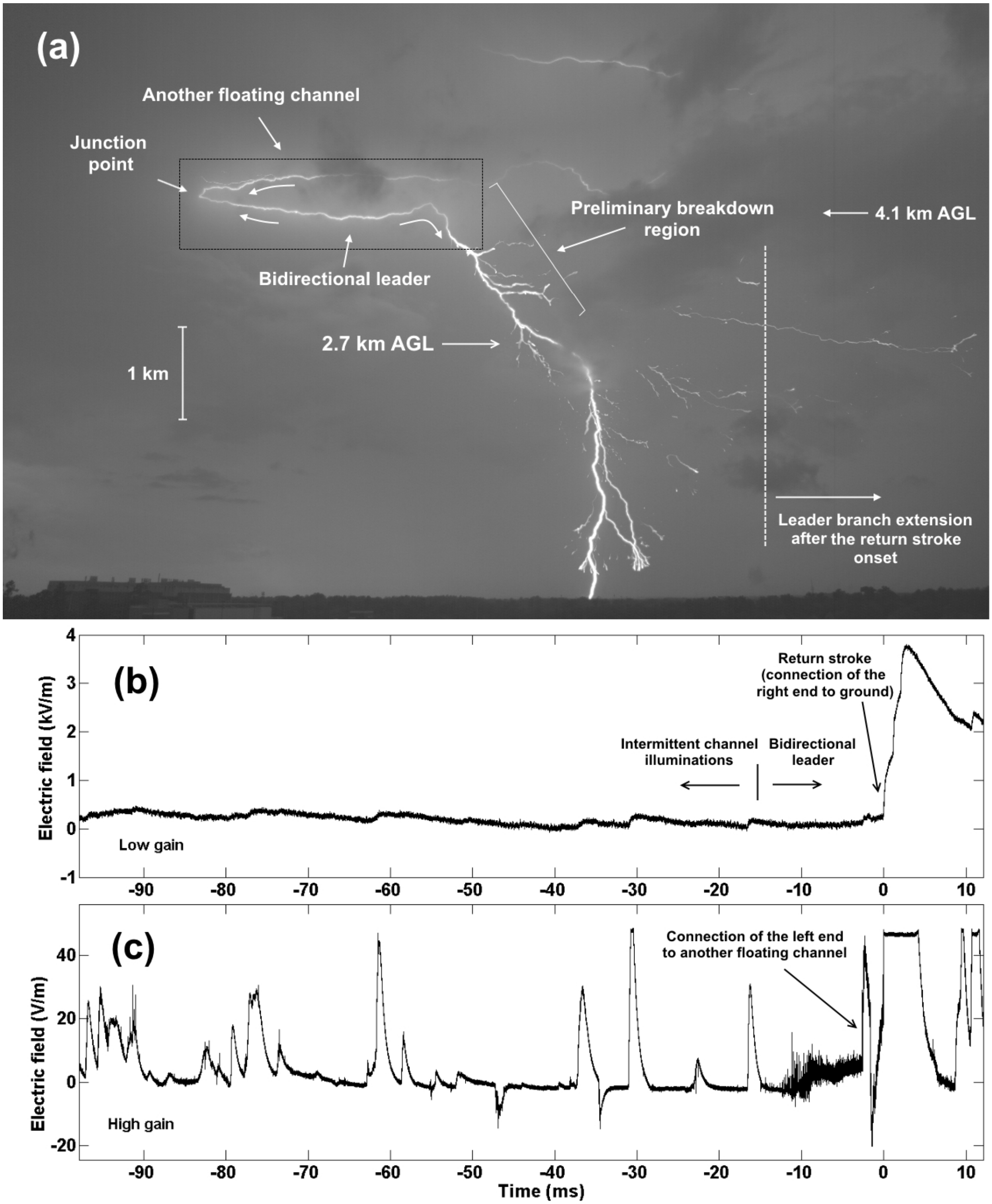

Fig. 1. (a) Composite image of 41 selected frames (from -123 to 9.8 ms) showing the bidirectional leader, another floating channel, and channel to ground. The high-speed video record started at -178 ms. (b-c) Low-gain and high-gain electric field records (from -98 to 12 ms), respectively. The right, negative end turned toward ground, likely due to the presence of positive charge between 4.1 and 2.7 km AGL. The left, positive end of the bidirectional leader made contact with another floating channel (the junction point is labeled in (a) and the electric field signature of the connection process is seen in (c)) prior to the right end's making contact with the ground. Adapted from Tran and Rakov (2016) [1].

leader extended in virgin for at least 12 m. Tran and Rakov (2016) [1] observed that the behavior of the positive end was drastically different from that of the negative end. Specifically, the positive end exhibited little variations in its extent, while the negative end extended steadily from about 4.1 km to 1 km above ground level (AGL). The return stroke occurred about 2.4 ms after the left end had come in contact with another floating channel (see "Junction point" in Figure 1a). The process of connecting the two floating channels caused saturation of the corresponding frame. The return stroke was followed by continuing current, whose duration (inferred from high-speed video images) was 21.9 ms.

The U.S. National Lightning Detection Network (NLDN) reported the distance between the ground termination of this cloud-to-ground stroke to the LOG to be 8.4 km. We used this distance for all points of interest on the luminous channel, which we assumed to be located on the plane that is perpendicular to the camera line of sight and contains the strike point. Based on this assumption, we estimated the distance errors to be between 20% and 30%. All the lengths and speeds presented in this paper are two-dimensional, and, hence, are likely to be underestimates (lower bounds) of actual values. The corresponding three-dimensional values are expected to be about 30% larger (Idone et al., 1984 [8]; Gao et al., 2014 [9]).

III. Electrostatic model of bidirectional leader

The electrostatic model presented here represents the development of our bidirectional leader between -11.1 and -2.7 ms. The positive end made connection to another floating channel at about -2.4 ms. Figures 2a and 2b are the composite images of frames before and during the time interval of interest. The corresponding channel representations in the model are shown in Figures 2c and 2d. The maximum extent of the positive end appeared to vary only slightly, while the negative end extended steadily in the 4.1 to 1.0 km height range.

Our electrostatic model is based on the assumptions given below.

1. The intermittent, predominantly horizontal cloud discharges that occurred during the time interval of interest insignificantly contributed to the electric field on the ground surface. This assumption is based on our modeling results which show that short horizontal floating channels produce negligible vertical electric field change at the ground level. For example, a 2-km long, horizontal bipolar channel, whose charge density slope is similar to that of the bidirectional leader (will be discussed later) produced a vertical electric field change of about 0.7 V/m vs. the measured net field change of 94 V/m (see Figure 3).
2. The polarity reversal (neutral) point was stationary between -11.1 and -2.7 ms and was located somewhere between the short positive branch labeled in Figure 2b and the first ground-bound turn of the negative end. In the model, we assumed that the neutral point was located at 0.75 km to the left from the negative-end turning point (see Figures 2c and 2d). The variation of the neutral-point location within the limits indicated above resulted in less than 9% difference in the total charge transfer.
3. The positive part of the bidirectional leader was essentially horizontal between -11.1 and -2.7 ms (see Figure 2b) and its length was set to 1.3 km. In order to satisfy the principle of conservation of charge, the slope of positive line charge density was made variable.
4. The negative part consisted of a horizontal, tilted, and vertical sections. The tilted section extended at angle $\alpha = 40^\circ$ with respect to vertical. Its junction point with the lowest, vertical section was 2 km AGL (see Figure 2d). The channel extension speeds are the frame-to-frame speeds estimated from the high-speed video record. The slope of line charge density along all three negative channel sections was assumed to be the same and not change with time from -11.1 to -2.7 ms.
5. The line charge density of the positive and negative parts was zero at the neutral point and linearly increased toward each of the channel extremities. The net charge on the entire bidirectional leader channel was zero at all times.
6. The transient-event channel, which occurred at -8.3 ms and increased the 2D length of the positive part by 0.35 km, was neglected since it resulted in less than 5% difference in the total charge transfer.

Figures 2c and 2d show the (x, y, z) coordinates of the extremities of the positive and negative parts, which are $(x^+, 0, z^+)$, and $(x^-, 0, z^-)$, respectively, all being in the xz vertical plane at $y = 0$. The origin of coordinates is set to the neutral point. z_0 and x_0 are the height of the neutral point and its distance to the ground-bound turning point of the negative end, respectively, which were varied to study the effect of uncertainties in distance measurements and in the assumed neutral point location.

In our model geometry shown in Figure 2, $z_0 = 4.1$ and $x_0 = 0.75$. The observation point is located at (-0.75, 8.4, -4.1) at the ground level, 8.4 km from the vertical plane. The coordinates of different points of interest including the extremities of the positive and negative ends at different times are given in Table I. The time step is set to 1 μs, so the length of leader segments, which were approximated by point charges, varied from 0.03 to 0.7 m, which is much smaller than the lengths of channel sections and the distance to the observation point.

TABLE I. Coordinates of the neutral point, observation point, and the extremities of the positive and negative ends, as seen in Figure 2

Point	Time/Time interval	Coordinates		
		x	y	z
Neutral point	-11.1 to -2.7 ms	0	0	0
Observation point		-0.75	8.4	-4.1
Positive end	-11.1 to -2.7 ms	1.3	0	0
Negative end	-11.1 ms	-1.1	0	-0.4
	-5.5 ms	-2.55	0	-2.1
	-2.7 ms	-2.55	0	-3.1
	0	-2.55	0	-4.1

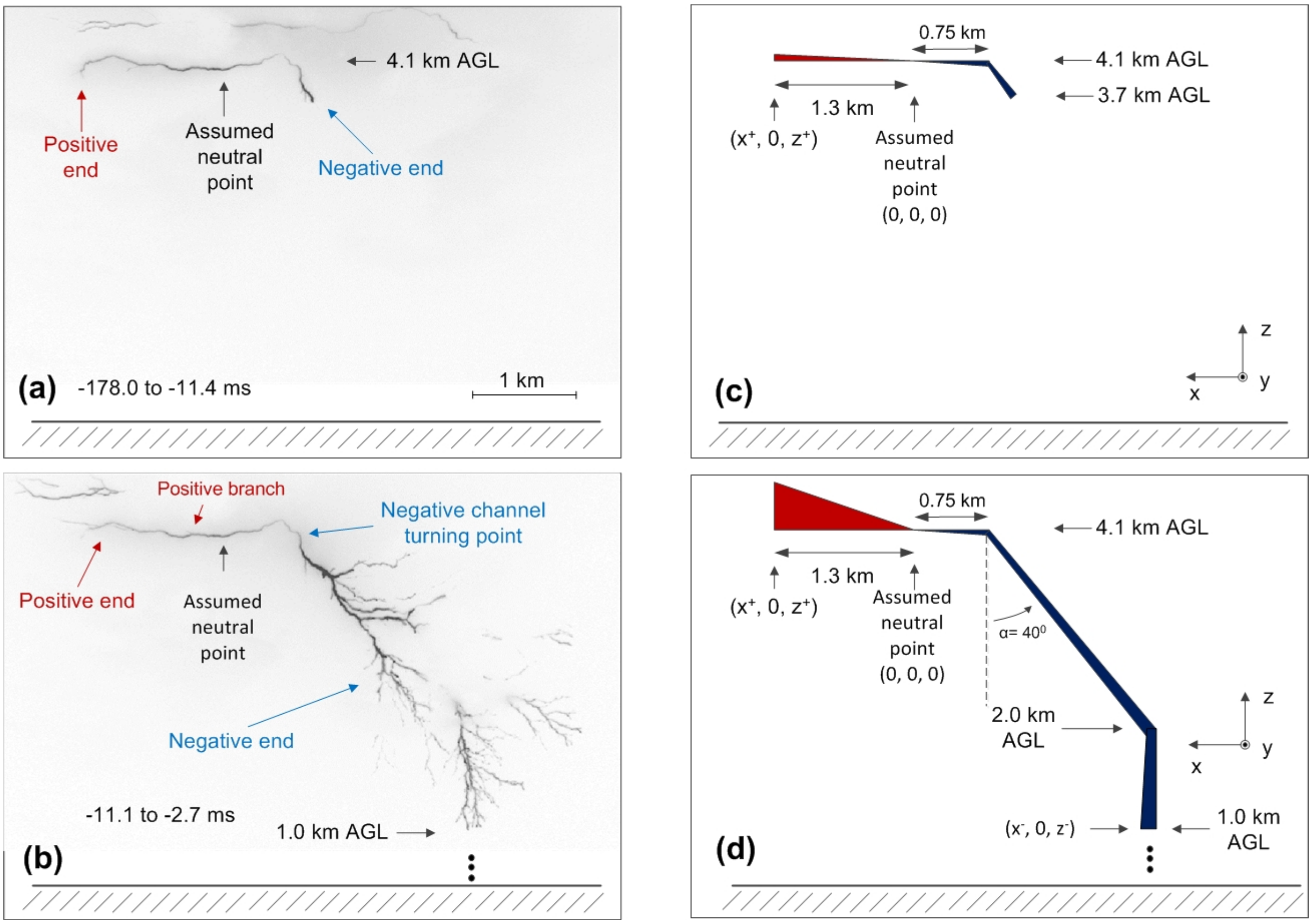

Fig. 2. (a) Composite image of all frames between -178 ms (the beginning of the high-speed video record) and -11.1 ms. (b) Composite image of frames between -11.1 and -2.7 ms (frame -8.3 ms containing the transient event is excluded), showing the negative end descending from 4.1 to 1.0 km. (c and d) Geometries of our electrostatic model at -11.1 and -2.7 ms, respectively. The neutral point is assumed to be stationary between the rightmost positive branch labeled in (b) and the ground-bound turn at the negative end. The line charge density is assumed to be linearly increasing from zero at the assumed neutral point to maxima at the extremities of the positive and negative leader channels.

The following labels are used in the model. l is the distance along the leader channel from differential segment dl to the neutral point. Superscripts $+$ and $-$ correspond to the positive and negative parts of the bidirectional leader. ρ, v, t, and L are the line charge density, leader speed, time, and channel length of the positive or negative part, respectively. The modeling steps are presented below.

- $v^-(t)$ is set to the frame-to-frame speed of the negative end estimated from the high-speed video record,
- $v^+(t) = 0$,
- $\rho^-(l^-) = k^-l^-$, where k^- is the slope of the negative line charge density distribution along the channel sections, which is varied to match the measured net electric field change,
- $\rho^+(l^+) = k^+l^+$, where k^+ is the slope of the positive line charge density distribution, which is found from the balance of charge at the positive and negative parts: $\int \rho^-(l^-)dl^- = -\int \rho^+(l^+)dl^+$.

At time t the vertical electric field at ground produced by an L-m long channel whose line charge density is $\rho(l,t)$ can be computed as (Rakov and Uman, 2003) [6]:

$$E(t) = \int_0^L \frac{\rho(l,t)H(l)dl}{2\pi\epsilon_0 R^3(l)} = \int_0^L \frac{\rho(l,t)H(l)dl}{2\pi\epsilon_0 (H^2(l)+D^2(l))^{1.5}}, \tag{1}$$

where $H(l)$, $D(l)$, and $R(l)$ are the height of differential channel segment dl and its horizontal and inclined distances to the observation point, respectively.

Applying equation (1) to the positive part and using:

$$L^+ = x^+,$$
$$H(l^+) = z_0,$$
$$D^2(l^+) = r^2 + (l^+ + x_0)^2,$$

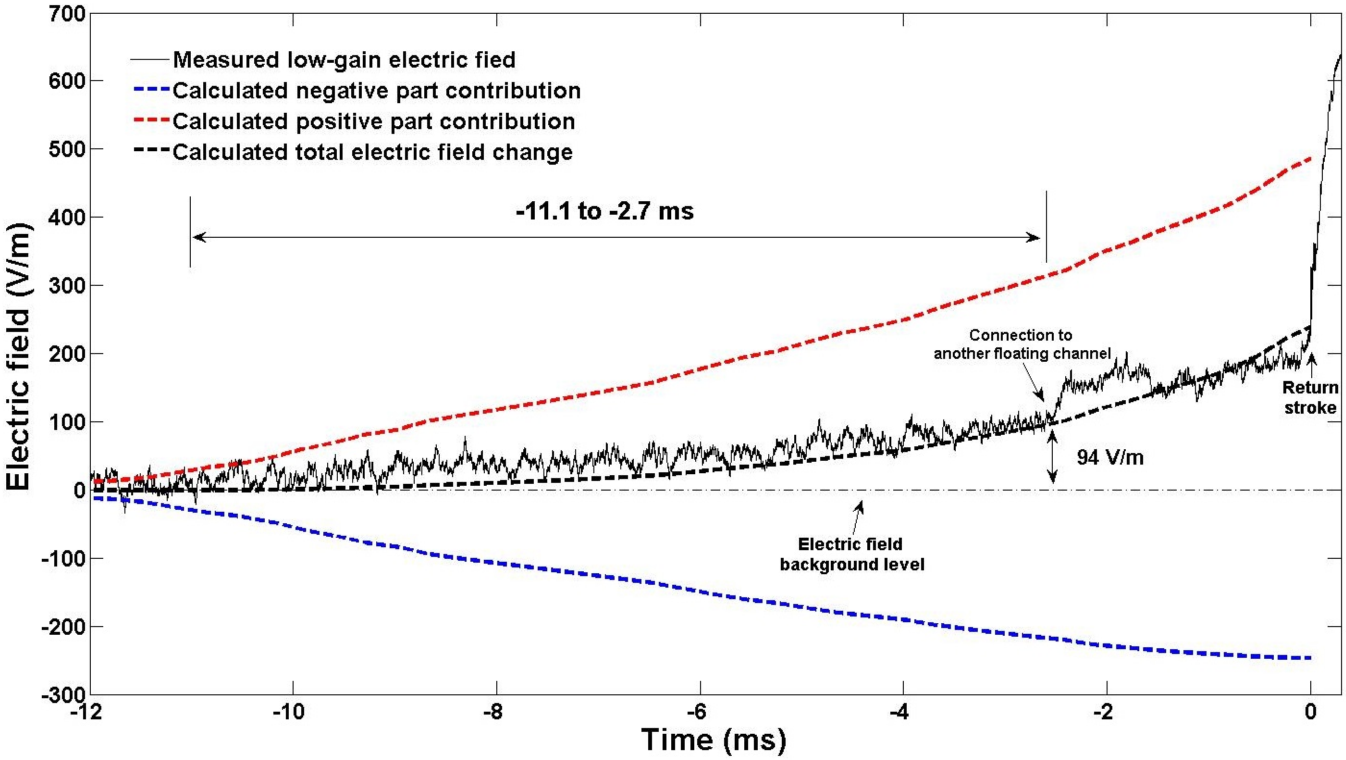

Fig. 3. Measured electric field (after compensation for instrumental decay) at 8.4 km vs. electric fields computed using the electrostatic model. The net electric field change between -11.1 and -2.7 ms is 94 V/m. The vertical electric field was measured at the LOG 8.4 km from the NLDN-reported ground termination.

$$E^+(t) = \int_0^{x^+} \frac{\rho^+(l^+,t)z_0 dl^+}{2\pi\epsilon_0(z_0^2+r^2+(l^++x_0)^2)^{1.5}}, \tag{2}$$

$$E^-(t) = \begin{cases} \displaystyle\int_0^{L^-(t)} \frac{\rho^-(l^-,t)z_0 dl^-}{2\pi\epsilon_0(z_0^2+r^2+(x_0-l^-)^2)^{1.5}} \text{ if } L^-(t) \le x_0, \\ \displaystyle\int_0^{x_0} \frac{\rho^-(l^-,t)z_0 dl^-}{2\pi\epsilon_0(z_0^2+r^2+(x_0-l^-)^2)^{1.5}} + \\ \displaystyle\int_{x_0}^{L^-(t)} \frac{\rho^-(l^-,t)(z_0-(l^--x_0)cos\alpha)dl^-}{2\pi\epsilon_0((z_0-(l^--x_0)cos\alpha)^2+r^2+((l^--x_0)sin\alpha)^2)^{1.5}} \text{ if } x_0 < L^-(t) \le x_0+2.1/cos\alpha, \\ \displaystyle\int_0^{x_0} \frac{\rho^-(l^-,t)z_0 dl^-}{2\pi\epsilon_0(z_0^2+r^2+(x_0-l^-)^2)^{1.5}} + \\ \displaystyle\int_{x_0}^{x_0+2.1/cos\alpha} \frac{\rho^-(l^-,t)(z_0-(l^--x_0)cos\alpha)dl^-}{2\pi\epsilon_0((z_0-(l^--x_0)cos\alpha)^2+r^2+((l^--x_0)sin\alpha)^2)^{1.5}} + \\ \displaystyle\int_{x_0+2.1/cos\alpha}^{L^-(t)} \frac{\rho^-(l^-,t)(z_0-2.1-(l^--x_0-2.1/cos\alpha))dl^-}{2\pi\epsilon_0((z_0-2.1-(l^--x_0-2.1/cos\alpha))^2+r^2+1.8^2)^{1.5}} \text{ otherwise.} \end{cases}$$

we obtained the following expression:

$$E^+(t) = \int_0^{L^+} \frac{\rho^+(l^+,t)H(l^+)dl^+}{2\pi\epsilon_0(H^2(l^+)+D^2(l^+))^{1.5}},$$
$$= \int_0^{x^+} \frac{\rho^+(l^+,t)z_0 dl^+}{2\pi\epsilon_0(z_0^2+r^2+(l^++x_0)^2)^{1.5}}.$$

The negative part is divided into three sections: horizontal, tilted, and vertical. The equation for horizontal section is applied when the length of the negative part is smaller than x_0 ($L^-(t) \le x_0$) and is derived using equation (1) as follows:

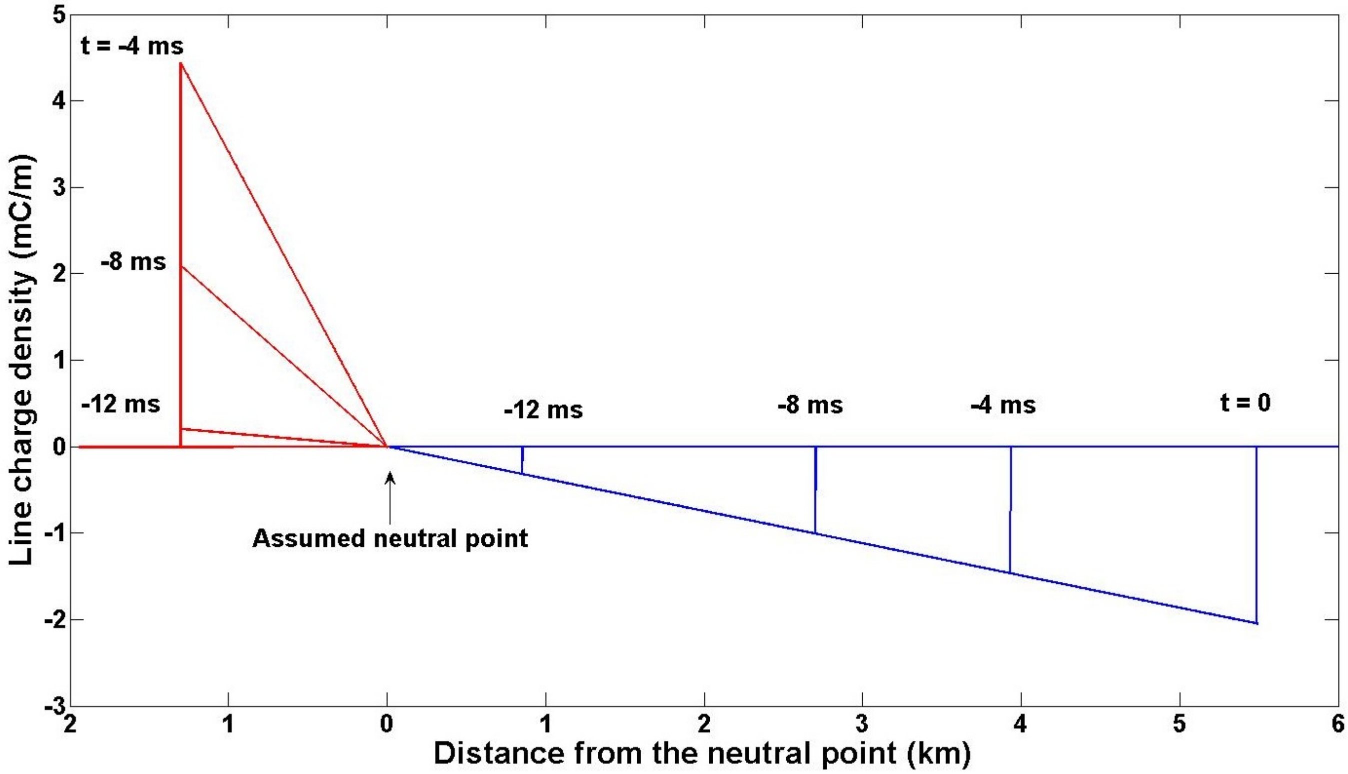

Fig. 4. Line charge density vs. scalar distance from the neutral point. Red and blue lines correspond to the positive and negative parts of the bidirectional leader, respectively, at 4 (negative end) or 3 (positive end) instants of time, starting from -12 ms with a time step of 4 ms. The slope of line charge density at the negative end is constant, while at the positive end it increases to keep the net charge on the leader channel equal to zero at all times. The positive line charge density at $t = 0$ is not shown because at -2.4 ms the positive end connected to another floating channel of unknown length.

$$
\begin{aligned}
L^-(t) &= \int_0^t v^- d\tau, \\
H &= z_0, \\
D^2(l^-) &= r^2 + (x_0 - l^-)^2, \\
E^-_{hor}(t) &= \int_0^{L^-(t)} \frac{\rho^-(l^-,t)H(l^-)dl^-}{2\pi\epsilon_0(H^2(l^-)+D^2(l^-))^{1.5}} \\
&= \int_0^{L^-(t)} \frac{\rho^-(l^-,t)z_0 dl^-}{2\pi\epsilon_0(z_0^2+r^2+(x_0-l^-)^2)^{1.5}}
\end{aligned}
$$

When $x_0 < L^-(t) < x_0{+}2.1/cos\alpha$, the equation for the tilted section is applied, which is derived as follows:

$$
\begin{aligned}
&L^-(t) = \int_0^t v^- d\tau, \\
&H(l^-) = z_0 - (l^- - x_0)cos\alpha, \\
&D^2(l^-) = r^2 + ((l^- - x_0)sin\alpha)^2, \\
&E^-_{til}(t) = \int_{x_0}^{L^-(t)} \frac{\rho^-(l^-,t)H(l^-)dl^-}{2\pi\epsilon_0(H^2(l^-)+D^2(l^-))^{1.5}} \\
&= \int_{x_0}^{L^-(t)} \frac{\frac{1}{2\pi\epsilon_0}\rho^-(l^-,t)(z_0-(l^- - x_0)cos\alpha)dl^-}{((z_0-(l^- - x_0)cos\alpha)^2+r^2+((l^- - x_0)sin\alpha)^2)^{1.5}}.
\end{aligned}
$$

When $x_0{+}2.1/cos\alpha < L^-(t)$, the equation for vertical section is applied, which is derived as follows:

$$
\begin{aligned}
&L^-(t) = \int_0^t v^- d\tau, \\
&H(l^-) = z_0 - 2.1 - (l^- - x_0 - 2.1/cos\alpha), \\
&D^2(l^-) = r^2 + (1.8)^2, \\
&E^-_{ver}(t) = \int_{x_0+\frac{2.1}{cos\alpha}}^{L^-(t)} \frac{\rho^-(l^-,t)H(l^-)dl^-}{2\pi\epsilon_0(H^2(l^-)+D^2(l^-))^{1.5}} \\
&= \int_{x_0+\frac{2.1}{cos\alpha}}^{L^-(t)} \frac{\frac{1}{2\pi\epsilon_0}\rho^-(l^-,t)(z_0-2.1-(l^- - x_0 - \frac{2.1}{cos\alpha}))dl^-}{((z_0-2.1-(l^- - x_0 - \frac{2.1}{cos\alpha}))^2+r^2+1.8^2)^{1.5}}.
\end{aligned}
$$

Equations for the electric fields produced by the positive and negative parts of the bidirectional leader are summarized in equation (2).

Frame-to-frame speeds of the negative end were not available before -14.9 ms and were assumed to be equal to the first measurable negative end speed. Extension of the negative leader before -11.1 ms produced only -1.3 V/m change vs. the total field change of 94 V/m. Thus, exclusion of the time interval before -11.1 ms does not materially change any of our results.

In the model, the net electric field change at the ground level is proportional to the charge density slope of the negative end. The proportionality coefficient was estimated to be

2.52×10^8 V×m/C. For the measured net electric field change of 94 V/m between -11.1 and -2.7 ms, the charge density slope was found to be 3.7×10^{-7} C/m^2. The computed and measured electric fields are in reasonably good agreement, as shown in Figure 3, where the contributions from the positive and negative parts are also given.

Figure 4 shows the charge density distribution along the two oppositely charged leader parts at different times, starting from -12 ms with a time step of 4 ms. At -2.7 ms, the line charge density at the negative leader extremity was -1.6 mC/m and the length of the negative leader was 4.4 km. At the other, positive end of the bidirectional leader, the line charge density was 5.5 mC/m. The contributions of the positive and negative ends to the total electric field at the ground were 310 and -216 V/m, respectively. From -11.1 to -2.7 ms, the charge transfer was 3.3 C, which resulted in an average current of 393 A. If the slope of negative charge density is assumed to remain the same until the leader attachment to ground and the increase of positive end length due to the connection to another floating channel is neglected, the total charge transfer Q will be 5.6 C. This is the charge deposited on the negative part of the bidirectional leader. If we assume that the charge neutralized by the return stroke is equal to that deposited on the negative part of bidirectional-leader channel, then according to the empirical formula relating the impulse charge transfer to the return-stroke peak current, $I = 10.6Q^{0.7}$ [Berger, 1972] [10], the corresponding peak current will be 35 kA similar to 36 kA estimated from radiation magnetic field peaks measured at multiple NLDN stations.

To study the effect of uncertainty in distance measurements, the height of the horizontal channel z_0 (see Figures 2c and 2d) was varied. Variation of the horizontal channel height within $\pm 30\%$ led to less than 13% change in the total charge transfer.

For comparison, if the positive part of the bidirectional leader were approximated by a time-varying point charge, the charge transfer and average current in the time interval of interest would be 3.0 C and 352 A, respectively. If, additionally, the negative end were assumed to be uniformly charged, the corresponding charge and current values would be 3.6 C and 429 A. All the values predicted by the simpler models are within 10% or so of their counterparts predicted by the more elaborate model presented in Figure 2.

The charge at the positive end is assumed to increase without channel extension, which implies that, for the assumed line charge density profile, the slope of the positive line charge density distribution increases with time. It is likely that the positive-end charge was leaking into the surrounding air via corona discharge on the lateral surface of the channel and via corona streamers at the positive leader extremity. Also, we cannot rule out a possibility of undetectable steady elongation of the positive end between -8.3 and -2.4 ms.

The average electric field in positive streamers E_r is about 500 kV/m (Bazelyan and Raizer, 2000) [11] and the longitudinal electric field is usually assumed to be negligible in comparison to the radial component (Maslowski and Rakov, 2006) [12]. By applying Gauss's law to a short channel segment with line charge density ρ, the radius of the corona sheath can be estimated as

$$r_{corona} = \frac{\rho}{2\pi\epsilon_0 E_r},$$

where ϵ_0 is the electric permittivity of free space. A channel section, whose line charge density is 5.3 mC/m, would have a corona sheath radius of 191 m.

Acknowledgment

This research was supported by NSF grant AGS-1701484. We would like to thank William Brooks of Vaisala Inc. for providing NLDN data.

References

[1] M. D. Tran and V. A. Rakov, "Initiation and propagation of cloud-to-ground lightning observed with a high-speed video camera," *Nature Scientific Reports*, vol. 6, no. 39521, 2016.

[2] J. Montanya, O. van der Velde, and E. R. Williams, "The start of lightning: Evidence of bidirectional lightning initiation," *Nature Scientific Reports*, vol. 5, p. 15180, 2015.

[3] T. A. Warner, M. M. F. Saba, C. Schumann, J. H. Helsdon, and R. E. Orville, "Observations of bidirectional lightning leader initiation and development near positive leader channels," *Journal of Geophysical Research: Atmospheres*, vol. 121, no. 15, pp. 9251–9260, 2016. [Online]. Available: http://dx.doi.org/10.1002/2016JD025365

[4] W. Rison, P. R. Krehbiel, M. G. Stock, H. E. Edens, X. M. Shao, R. J. Thomas, M. A. Stanley, and Y. Zhang, "Observations of narrow bipolar events reveal how lightning is initiated in thunderstorms," *Nature Communications*, vol. 7, p. 10721, 2016.

[5] N. Liu *et al.*, "Streamer Interpretation of Fast Breakdown in Narrow Bipolar Event," in *1st International Symposium on Lightning Physics and Lightning Meteorology*, Beijing, China, September 2017.

[6] V. A. Rakov and M. A. Uman, *Lightning: Physics and Effects*. Cambridge University Press, New York, 2003. [Online]. Available: http://books.google.com/books?id=NviMsvVOHJ4C

[7] V. Mazur and L. H. Ruhnke, "Common physical processes in natural and artificially triggered lightning," *Journal of Geophysical Research: Atmospheres*, vol. 98, no. D7, pp. 12 913–12 930, 1993.

[8] V. P. Idone, R. E. Orville, P. Hubert, L. Barret, and A. Eybert-Berard, "Correlated observations of three triggered lightning flashes," *Journal of Geophysical Research: Atmospheres*, vol. 89, no. D1, pp. 1385–1394, 1984. [Online]. Available: http://dx.doi.org/10.1029/JD089iD01p01385

[9] Y. Gao, W. Lu, Y. Ma, L. Chen, Y. Zhang, X. Yan, and Y. Zhang, "Three-dimensional propagation characteristics of the upward connecting leaders in six negative tall-object flashes in Guangzhou," *Atmospheric Research*, vol. 149, pp. 193 – 203, 2014.

[10] K. Berger, "Methoden und Resultate der Blitzforschung auf dem Monte San Salvatore bei Lugano in den Jahren 1963-1971," *Bull. Schweiz. Elektrotech. Ver.*, vol. 63, pp. 1403 – 22, 1972.

[11] E. M. Bazelyan and Y. P. Raizer, *Lightning Physics and Lightning Protection*. Bristol: IOP Publishing, London, UK, 2000.

[12] G. Maslowski and V. A. Rakov, "A study of the lightning channel corona sheath," *Journal of Geophysical Research: Atmospheres*, vol. 111, no. D14, 2006. [Online]. Available: http://dx.doi.org/10.1029/2005JD006858